Conformational plasticity of the type I maltose ABC importer

Simon Böhm[a,1], Anke Licht[b,1], Steven Wuttge[b], Erwin Schneider[b,2], and Enrica Bordignon[a,2]

[a]Laboratory of Physical Chemistry, Eidgenössische Technische Hochschule Zurich, 8093 Zurich, Switzerland; and [b]Institut für Biologie/Bakterienphysiologie, Humboldt-Universität zu Berlin, 10115 Berlin, Germany

Edited by G. Marius Clore, National Institute of Diabetes and Digestive and Kidney Diseases, National Institutes of Health, Bethesda, MD, and accepted by the Editorial Board February 21, 2013 (received for review October 12, 2012)

ATP-binding cassette (ABC) transporters couple the translocation of solutes across membranes to ATP hydrolysis. Crystal structures of the *Escherichia coli* maltose importer ($MalFGK_2$) in complex with its substrate binding protein (MalE) provided unprecedented insights in the mechanism of substrate translocation, leaving the MalE–transporter interactions still poorly understood. Using pulsed EPR and cross-linking methods we investigated the effects of maltose and MalE on complex formation and correlated motions of the $MalK_2$ nucleotide-binding domains (NBDs). We found that both substrate-free (open) and liganded (closed) MalE interact with the transporter with similar affinity in all nucleotide states. In the apo-state, binding of open MalE occurs via the *N*-lobe, leaving the C-lobe disordered, but upon maltose binding, closed MalE associates tighter to the transporter. In both cases the NBDs remain open. In the presence of ATP, the transporter binds both substrate-free and liganded MalE, both inducing the outward-facing conformation trapped in the crystal with open MalE at the periplasmic side and NBDs tightly closed. In contrast to ATP, ADP–Mg^{2+} alone is sufficient to induce a semi-open conformation in the NBDs. In this nucleotide-driven state, the transporter binds both open and closed MalE with slightly different periplasmic configurations. We also found that dissociation of MalE is not a required step for substrate translocation since a supercomplex with MalE cross-linked to MalG retains the ability to hydrolyze ATP and to transport maltose. These features of MalE–$MalFGK_2$ interactions highlight the conformational plasticity of the maltose importer, providing insights into the ATPase stimulation by unliganded MalE.

ATP-binding cassette (ABC) systems are found in all kingdoms of life, forming one of the largest protein superfamilies (1–4). ABC transporters comprise two transmembrane domains (TMDs) that form the translocation pathway and two nucleotide-binding domains (NBDs) that bind and hydrolyze ATP. Based on biochemical and structural evidence, all ABC transporters are thought to function by an "alternate-access" mode, with the translocation path shuttling between an inward-facing and outward-facing conformation in response to substrate and ATP binding, the latter causing the NBD dimer to close (5).

Canonical ABC importers are subdivided into type I and type II based on structural and biochemical evidence (6) and are dependent on extracellular (or periplasmic) substrate binding proteins (SBPs) (4), which play a crucial role in initial steps of the transport cycle (7–10). SBPs generally consist of two symmetrical lobes that rotate toward each other upon substrate binding (11).

The type I maltose transporter of *Escherichia coli*/*Salmonella* is probably the best understood ABC transporter to date (12). It is composed of the periplasmic maltose binding protein, MalE, the membrane-integral subunits, MalF and MalG, and the nucleotide-binding subunits (NBDs), $MalK_2$. The available crystal structures in the pretranslocation, ATP-, and vanadate-trapped states (13–16) have largely contributed to the understanding of the details of the inward- to outward-facing mechanism. The posthydrolytic state has not yet been crystallized, but data exist proposing this state to have a distinct structure from the other three known crystal snapshots (8, 9). MalE interacts with the transporter throughout the nucleotide cycle (15–18), and the X-ray structures revealed the switch of the binding protein from the liganded (closed) to the substrate-free (open) conformation concomitantly with ATP binding to the NBDs. Despite all these structural insights, the response of the transporter to substrate availability is poorly understood. Furthermore, the mechanism behind the stimulation of the ATPase activity of the transporter by unliganded MalE (10, 19) is still elusive (20, 21).

Our results show that the apo- and ADP-states of the transporter bind both open and closed MalE, but the complex adopts different periplasmic configurations. The ATP-state of the transporter can bind either closed MalE, inducing its opening and release of substrate to MalF or directly unliganded MalE, which generates a futile cycle. In both cases the NBDs are triggered into a fully closed dimer primed for ATP hydrolysis. Furthermore, we demonstrate that dissociation of the binding protein is not a prerequisite for substrate translocation. These features highlight the conformational plasticity of a type I ABC importer.

Results

Experimental System and Techniques Used. We performed chemical cross-linking and EPR spectroscopy in detergent-solubilized and reconstituted transporters to detect MalE–MalG and MalK–MalK distances between cysteines or spin-labeled cysteines [labeled with MTSL, (1-Oxyl-2,2,5,5-tetramethylpyrrolidin-3-yl) methyl methanethiosulfonate label] shown in Fig. 1. The cys mutations and subsequent labeling did not affect ATPase activity of the variants (Table S1). Site-directed chemical cross-linking was performed using flexible homobifunctional thiosulfonate linkers with defined spacer lengths in the extended conformation of 5.2 Å (1,2 ethanediyl-bismethanethiosulfonate, EBS), 10.4 Å (1,6 hexandiyl-bismethanethiosulfonate, HBS), and 24.7 Å (3,6,9,12,15-pentaoxaheptadecan-1,17-diyl-bis-methanethiosulfonate, PBS) (22). Mean distances and distance distributions between singly spin-labeled MalE and singly labeled $MalFGK_2$ and between doubly spin-labeled NBDs were obtained by double electron–electron resonance (DEER) at cryogenic temperatures, which provides a "frozen" snapshot of the equilibrium population of the complex. As an example of the complementarity and reliability of the two methods, Fig. 1*B* shows the agreement between experimental distance constraints obtained in the apo-state of the complex by DEER or cross-linking and the simulations performed on the corresponding crystal structure [Protein Data Bank (PDB) 3PV0].

Maltose- and Nucleotide-Mediated Interaction Between MalE and MalG. Cross-linking between P78C (amino acids are designated by the

Author contributions: E.S. and E.B. designed research; S.B., A.L., S.W., and E.B. performed research; S.B., A.L., E.S., and E.B. analyzed data; and S.B., A.L., E.S., and E.B. wrote the paper.

The authors declare no conflict of interest.

This article is a PNAS Direct Submission. G.M.C. is a guest editor invited by the Editorial Board.

[1]S.B. and A.L. contributed equally to this work.

[2]To whom correspondence may be addressed. E-mail: erwin.schneider@biologie.hu-berlin.de or enrica.bordignon@phys.chem.ethz.ch.

This article contains supporting information online at www.pnas.org/lookup/suppl/doi:10.1073/pnas.1217745110/-/DCSupplemental.

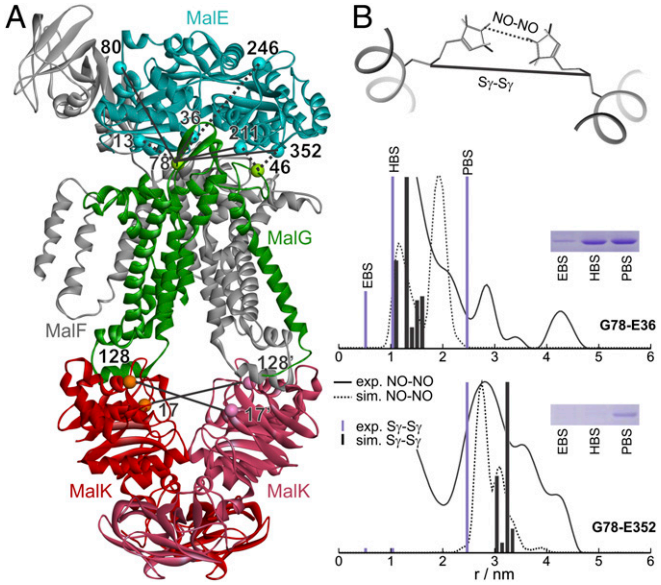

Fig. 1. DEER and cross-linking distance restraints vs. MalFGK$_2$-E structure. (*A*) Apo-state crystal structure [Protein Data Bank (PDB) 3PV0]. The Cα atoms of the residues replaced by cysteines in this study are shown in ball representation. Some pairs were chosen for both cross-linking and DEER measurements (solid lines), others only for cross-linking (dotted lines). (*B*) Experimental DEER (straight black line) and cross-linking (violet bar) distances obtained with the pairs G78-E36 and G78-E352 (the letters denote the subunit of the site) compared with the simulated nitroxide–nitroxide (NO–NO, dotted line) and sulfur–sulfur (Sγ–Sγ, black bar) distances simulated with MMM using spin-labeled rotamers (MTSL library at 175 K) on the structure 3PV0. The insets show the corresponding bands in the gel.

one-letter code throughout) in MalG and two cysteines placed in the *N*-lobe of MalE was performed to follow complex formation under different conditions. In the presence of MalE(G13C) a strong cross-link to MalG(P78C) was found with all linkers (marked EG in Fig. 2*A*), regardless of the presence of maltose and/or nucleotides. This agrees with the available crystal structures (13, 15) that show no significant change in the Cα–Cα distance between both residues in different nucleotide states (Table S2) and confirms that both open and closed MalE bind to the transporter. The results were confirmed in proteoliposomes, thus strongly indicating that the properties of the detergent-solubilized maltose transport complex reflect those in lipid environment (Fig. S1*A*). The cross-link between MalG(P78C) and another Cys in the *N*-lobe of MalE (position 36) was likewise found to be independent of maltose (Fig. S1*C*). Reliability and specificity of this approach were validated using a Cys at position 246 in MalE located 3.3 nm apart from MalG(P78C) (Fig. 1*A*), which showed no cross-linking under any condition as expected (Fig. S2*C*). Moreover, reducing the incubation time with the cross-linker to 5 s, lowering the concentration of the cross-linker to 1 μM and of MalE to 1/8 relative to MalFGK$_2$ still resulted in a cross-linked product (Fig. S2 *A* and *B*). In contrast, the formation of MalE dimers by simple collision was found to be clearly dependent on MalE concentration (Fig. S2*B*).

DEER measurements were performed to extract accurate interspin distances between MalG(78R1) (with R1 being the spin-labeled side chain) and spin-labeled sites in the *N*-lobe of MalE. A broad distance distribution centered at 4 nm was measured between MalG(78R1) and position 80 in MalE in the apo-state (Figs. 2*B* and S3) independent of maltose. In the presence of 3 mM ATP (with additional 0.075 mM EDTA to abolish hydrolysis), the distance decreased to 3.8 nm, again independent of maltose (Fig. 2*B*). In the ADP-state (3mM ADP, 5 mM $MgCl_2$), in the presence and absence of maltose, two distinct distance distributions were measured, centered at 3.3 or 4 nm, respectively (Fig. 2*B*), demonstrating the role of the substrate for the periplasmic configuration of the *N*-lobe. The data confirmed that the ADP-state of the complex differs from both the apo- and ATP-snapshots (Fig. S3*C*). The interspin distance between MalG(78R1) and another spin label at position 36 in MalE was found to be below 2 nm (borderline region of DEER sensitivity); thus, only the apo-state was measured and the distance was found to be unaffected by maltose, corroborating the cross-linking findings (Fig. S3*A*). It is worth noting that the low modulation depth (0.1–0.2) observed in all DEER traces is to be attributed to the similar low affinity of MalE for the transporter in the three states investigated ($K_d \sim 10^{-4}$ M). The availability of a homemade high-power Q-band spectrometer allowed reliable detection of the DEER traces with optimal signal-to-noise and dipolar evolution time (23).

In response to maltose, the relative displacement between residues in the C-lobe of MalE (positions 211 and 352) and MalG was remarkably different from those in the *N*-lobe. From the crystal structures, the Cα–Cα distance between MalG(P78) and MalE(S352) changes from 3.4 to 4.2 nm going from the pretranslocation to the ATP-bound state (Table S2). A cross-linked product was observed with PBS in the apo-state, which was significantly enhanced (1.6-fold, four independent measurements) upon binding of maltose (Fig. 3*A*). We suggest a weak interaction between the C-lobe of unliganded MalE and the transporter, which is strengthened by maltose presence. Upon addition of ATP or in the vanadate-trapped state, no cross-linked product was obtained, independent of maltose, suggesting a shift of the C-lobe away from position 78 in MalG, consistent with the crystal data (13). The weak interaction of the C-lobe of MalE was restored by ATP hydrolysis and remained unchanged in the presence of ADP (Fig. 3*A*). These results were reproduced in proteoliposomes (Fig. S1*B*) and were corroborated with other pairs in MalG and in the C-lobe of MalE (Fig. S1 *D*–*F*).

The distance distributions obtained by DEER between spin labels attached at position 352 in the C-lobe of MalE and position 78 in MalG (Fig. 3*B* and Fig. S3) substantiate the cross-linking information. In fact, the C-lobe interaction in the pretranslocation state shows remarkable substrate dependence as revealed by the change from a broad (3–6 nm) to a narrower distance distribution (centered at 2.8 nm) upon maltose binding to MalE (Fig. 3*B*). Interestingly, in the ATP-state, a unique 4 nm mean distance was measured independent on maltose (Fig. 3*B*). In contrast to the *N*-lobe, in the ADP-state the C-lobe adopts the same relative position with respect to MalG independent of substrate (Fig. 3*B*). The maltose-dependent interactions in the pretranslocation state were further validated using a second position in the C-lobe (Fig. S3*A*) and the results obtained between MalG(P78R1) and MalE (S352R1) were confirmed in proteoliposomes (Fig. S4).

Notably, all experimental interspin distances between MalE and the reporter position 78 in MalG in the apo-state (with closed MalE) and in the ATP-state (with both MalE variants) agree well with those simulated using the program MMM (24) on the corresponding crystal structures (Figs. S3 and S4).

In summary, the data show that apo- and ADP-states of the transporter are not selective for open or closed MalE and that the complex has different periplasmic configurations in the absence or presence of substrate. In contrast, the ATP-state of the transporter can bind either closed MalE, switching it into the open conformation, or directly unliganded open MalE.

Effects of Maltose and MalE on the Conformation of the NBDs. The observed maltose effects on the interactions between MalE and MalFGK$_2$ prompted us to investigate whether maltose has an effect also on the NBDs' motions. Two cysteine mutations in the MalK helical domains (V17C and E128C) were introduced close to positions already used in a previous study (9). The 17–128′ (the prime denotes the second MalK monomer) and the 128–17′

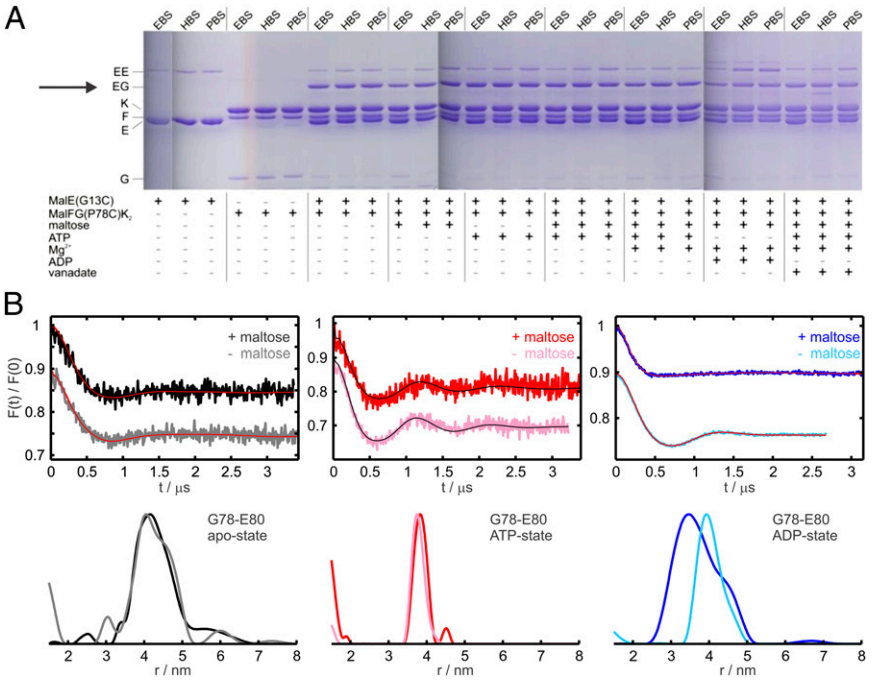

Fig. 2. Cross-linking and DEER data between MalFG(P78C)K_2 and sites in the *N*-lobe of MalE. (*A*) MalFG(P78C)K_2 in DDM micelles (2.5 μM) was incubated with MalE(G13C) (5 μM) and homobifunctional thiosulfonate cross-linkers (1 mM) in the presence of different cofactors as indicated. The cross-linked products were subsequently analyzed by SDS/PAGE. The cross-linkers EBS, HBS, and PBS have approximate spacer lengths of 5.2 Å, 10.4 Å, and 24.7 Å (see *SI Materials and Methods* for more details). (*B*) DEER analysis on MalFGK$_2$ transporters solubilized in n-Dodecyl β-D-maltoside carrying the spin label at position 78 in MalG incubated with MalE spin-labeled at the *N*-lobe (position 80) in different nucleotide states in the presence and absence of maltose, as indicated. (*Upper*) Normalized DEER Form factors F(t). (*Lower*) Distance distributions obtained with Tikhonov regularization using the software DeerAnalysis2011 (35). The mutants are denoted by the name of the relative subunit (e.g., G or E) and the corresponding residue number.

distances are distinctly shorter than all other intra- and inter-MalK distances and should report closure and reopening of the NBDs, according to the crystal structures. The apo-state of the MalFGK$_2$ alone (Fig. 4*A*, turquoise trace) showed a distance peak centered at 3.5 nm, which was associated with the 17–128′ and 17′–128 distances. Binding of open (Fig. 4*A*, gray) or closed (Fig. 4*A*, black) MalE only slightly affected this distance, indicating that the binding of MalE to the periplasmic side of the transporter does not alter the relative position of the open NBDs. Binding of ATP alone to MalFGK$_2$ did not close the NBDs (Fig. 4*B*, orange trace), in agreement with previous EPR studies (9). Only after MalE binding (independent of maltose) was the full closure of the NBDs observed, resulting in a mean distance centered at about 2.5 nm (Fig. 4*B*, red and pink traces).

Interestingly, we found that binding of ADP–Mg^{2+} to MalFGK$_2$ induced a semi-open conformation of the NBDs with a mean interspin distance of about 3 nm (brown trace in Fig. 4*C* and Fig. S5*A*), which was unaffected by subsequent binding of open or closed MalE (blue and cyan traces in Fig. 4*C* and Fig. S5 *B* and *C*). The latter findings highlight that this NBD's conformation is purely nucleotide-driven. In contrast, the ATP-state of the NBDs is driven by both MalE and ATP, and the complex adopts a unique conformation independent of maltose. The experimental distances show good agreement with those simulated on the available crystal structures (Fig. S5).

Cross-linking data performed on the MalE–MalFGK(V117C, E128C)$_2$ complex (Fig. S6) confirmed the MalE/nucleotide-driven NBD motions independent of maltose.

***N*-Lobe of MalE Requires Conformational Freedom for Substrate Import.** How important are the different periplasmic configurations of MalE for substrate import? And is the dissociation of MalE during the nucleotide cycle required for substrate transport? To address these questions, we created supercomplex variants containing PBS (~25 Å)-linked MalFG(P78C)K_2–MalE(G13C) and MalFG(T46C)K_2–MalE(S352C), representing linkage of the *N*- and C-lobes of MalE to the transporter, respectively. The supercomplexes were passed through a molecular sizing column to remove excess MalE and subsequently analyzed for ATPase activity and maltose transport. Both variants displayed ATPase activities comparable to those in the presence of freely diffusible MalE at a 1:1 molar ratio under the same conditions (Fig. 5*A*). However, and unlike the control, addition of excess soluble MalE to the cross-linked complex did not increase activity, suggesting a lack in space to accommodate more than one copy of MalE in the vicinity of the transport complex. The two supercomplex variants were also shown to retain the ability to transport maltose with similar efficiency as the complex in the presence of a 1:1 molar ratio of MalE (Fig. 5*B*). Thus, we conclude that dissociation is not a necessary requirement for transport. Strikingly, we found that the activity of a supercomplex was affected by the spacer length of the cross-linker. When linked by EBS (~5 Å), the complex containing MalG(P78C)–MalE(G13C) exhibited only basal ATPase activity (Fig. 5*A*) and showed no substrate transport (Fig. 5*B*), suggesting that the *N*-lobe's conformational freedom in the periplasmic region of the complex is required to accomplish the switch from the outward- to the inward- facing state leading to substrate import.

Discussion

Site-directed chemical cross-linking and DEER spectroscopy were applied to investigate the substrate dependency of the MalE–transporter interactions in different nucleotide states and the stimulatory effect of liganded and substrate-free MalE on the ATPase activity of the transporter.

In an intact *E. coli* cell and under inducing conditions of the maltose regulon, a 30–50-fold excess of MalE was observed relative to its membrane partners. However, only 20% of the normal MalE amount was required for full transporter activity (25), indicating that the high concentration of MalE in the periplasm is not mechanistically essential for transport. Our results corroborate this notion as cross-linked products and DEER traces were observed at only twofold excess of MalE over transporter, which allowed 70% of ATPase activity compared to a 10-fold excess. Moreover, we found that dissociation of MalE is not a necessary step to accomplish the full nucleotide cycle, as supercomplexes formed by cross-linking MalE and MalG with long linkers (PBS) showed normal ATPase activity and substrate transport. However, the conformational freedom of MalE in the periplasmic region of the complex is necessary for transport; in fact, blocking the

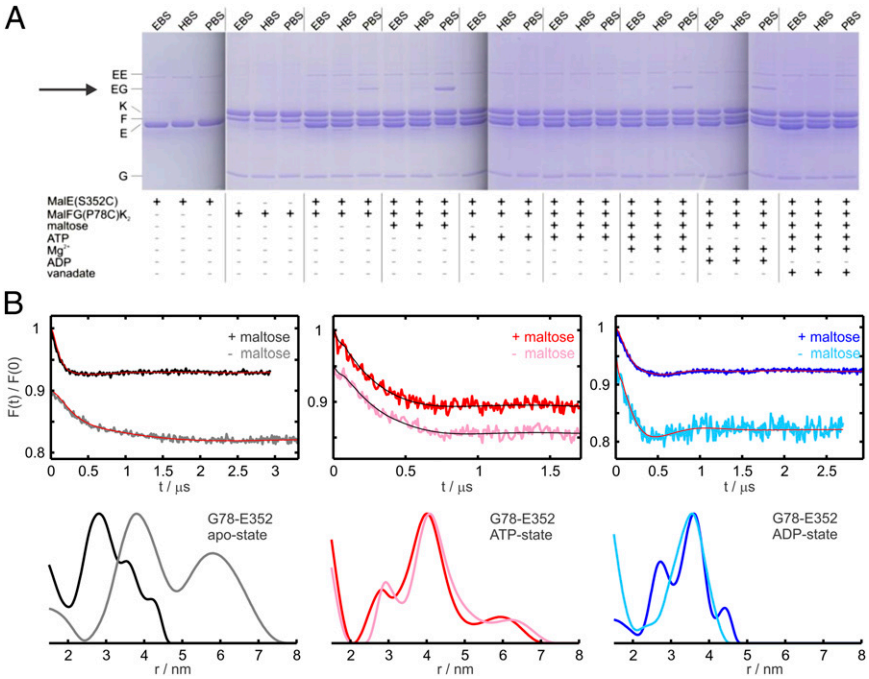

Fig. 3. Cross-linking and DEER data between MalFG(P78C)K_2 and sites in the C-lobe of MalE. (*A*) MalFG(P78C)K_2 in DDM micelles (2.5 μM) was incubated with MalE(S352C) (5 μM) and homobifunctional thiosulfonate cross-linkers (1 mM) in the presence of different cofactors as indicated. (*B*) DEER analysis on MalFGK_2 transporters solubilized in DDM carrying the spin label at position 78 in MalG incubated with MalE spin-labeled at the C-lobe (position 352) in different nucleotide states in the presence and absence of maltose, as indicated. (*Upper*) Normalized DEER Form factors F(t). (*Lower*) Distance distributions obtained with Tikhonov regularization using the software DeerAnalysis2011 (35). The mutants are denoted by the name of the relative subunit (e.g., G or E) and the corresponding residue number.

N-lobe movements with a short linker (EBS) abolished ATPase activity and transport. This finding is reminiscent of type I ABC importers with one or two solute-binding domains fused to one TMD (26). The analysis of such a transporter, the OpuA complex of *Lactococcus lactis*, revealed that two SBPs cooperatively interact but one is sufficient for transport (27).

Both in the presence and absence of substrate, three distinct conformations of the periplasmic region of the complex could be identified in the apo-, ATP-, and ADP-states. The almost constant low modulation depth in the DEER traces suggests that the affinity of MalE for the transporter stays in the 10^{-4} M range in the three states investigated and it is independent of maltose, in contrast to the nanomolar affinity between open MalE and the AMP–PNP (adenylylimidodiphosphate) state of MalFGK_2 reported recently (28).

Notably, we found that the structure of the MalE–transporter complex in the periplasmic region differs if MalE is added in the unliganded or maltose-loaded form to the apo- or ADP-state of the transporter. The interspin distances simulated on the X-ray structure of the complex in the pretranslocation state (15) are in good agreement only with the experimental distances in the presence of maltose (Figs. S3 and S4). In line with the finding that the ADP-structure of the complex differs from that in the apo-state, we found a different behavior of the *N*- and C-lobes of MalE upon maltose addition: in the ADP-state, the interaction with the C-lobe of MalE is unaffected, but the *N*-lobe adopts a slightly different conformation depending on substrate.

Schematic models of the different conformations monitored by EPR and cross-linking are depicted in Fig. 6 superimposed to the available structural data. In summary, the apo-state of the

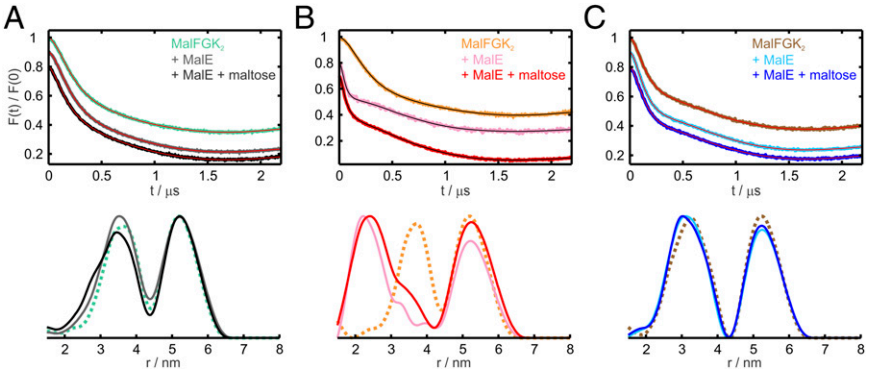

Fig. 4. MalE and maltose effects on MalK_2 interspin distances in different nucleotide states. (*Upper*) Normalized DEER Form factors F(t). (*Lower*) Distance distributions obtained with Tikhonov regularization using the software DeerAnalysis2011 (35) on MalFGK_2 transporters solubilized in DDM spin-labeled at positions 17 and 128 in MalK. The short distance peak (< 4.5 nm) represents the 17–128′ and 128–17′ contributions. (*A*) Apo-state of the MalFGK_2 transporters alone (turquoise) and after incubation with wild-type MalE in the absence (gray) and in the presence (black) of maltose. (*B*) Analogous DEER analysis performed in the presence of 10 mM AMP–PNP and 10 mM $MgCl_2$. MalFGK_2 transporters without MalE/maltose (orange) and incubated with WT–MalE in the absence (pink) and presence (red) of maltose. (*C*) Analogous DEER analysis performed in the presence of 10 mM ADP, 10 mM $MgCl_2$. MalFGK_2 transporters without MalE/maltose (brown) and incubated with WT–MalE in the absence (cyan) and in the presence (blue) of maltose. For clarity, the distance distribution obtained with the MalFGK_2 transporters alone are presented as dotted lines. The primary data and the distances simulated with MMM on the corresponding crystal structures are shown in Fig. S5.

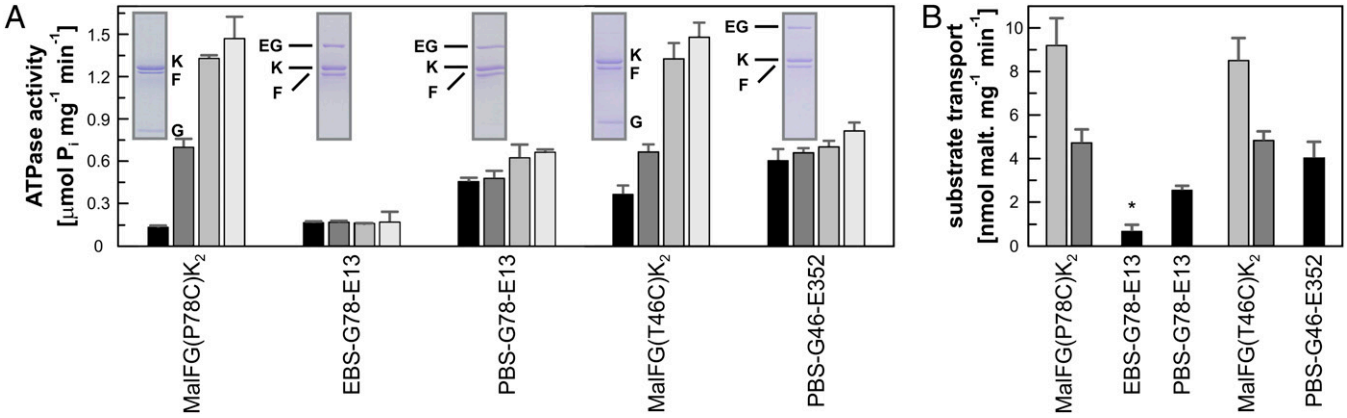

Fig. 5. ATPase and transport activities of cross-linked MalE–FGK_2 supercomplexes. (*A*) ATPase activity of MalFG(P78C), EBS-, or PBS-linked MalFG(P78C)–MalE (G13C) (named EBS-G78-E13, PBS-G78-E13) in the presence of increasing concentration of freely diffusible MalE(G13C) and of MalFG(T46C) and PBS-linked MalFG(T46C)–MalE(S352C) (named PBS-G46-E13) in the presence of increasing concentration of freely diffusible MalE(S352C). (*B*) [^{14}C]maltose transport of reconstituted MalFG(P78C) and MalFG(T46C) with added MalE(G13C) and MalE(S352C), respectively, at molar ratios 10:1 (gray) or 1:1 (dark gray) and of the supercomplexes EBS-G78-E13, PBS-G78-E13, and PBS-G46-E352. The asterisks in the EBS-linked supercomplex denote the observed basal maltose incorporation, with no time-dependent increase. Each value is the mean of three separate determinations with SD shown as error bars.

transporter, with open NBDs, binds the *N*-lobe of unliganded (open) MalE, while the C-lobe is more disordered. The presence of maltose leads to a tighter interaction between the C-lobe and the transporter, leaving the NBDs unaffected. Binding of ATP alone does not affect the ABC cassettes, but the concomitant presence of either open or closed MalE induces the full closure of the MalK dimer and the complex resembles the ATP crystal structure (Fig. S3*B* and S5*B*) (13, 15). Closed NBDs are primed to hydrolyze ATP, which explains the observed stimulation of ATPase by open MalE. We thus exclude that the observed stimulation by open MalE is due to the small fraction of closed MalE in equilibrium (20). The different conformations adopted during the remaining steps of the cycle in the periplasmic region of the complex are suggested to decrease the efficiency of the hydrolysis (Fig. 6*B*).

Hydrolysis of ATP switches the NBDs to a semi-open conformation, reintroducing the maltose-dependent interactions in the periplasmic region of the complex. The semi-open NBDs' conformation is found here to be purely nucleotide-driven; namely, ADP–Mg^{2+} is sufficient to induce the partial closure of the ABC cassettes in the absence of MalE (Fig. 6*A*). This is remarkably different from the negligible distance changes induced by ATP (or AMP–PNP–Mg^{2+}) between positions 17 and 128 introduced as reporter side chains in MalK, in agreement with previous EPR studies (9). It is worth mentioning that a partial closure was observed by EPR and cross-linking upon ATP binding in the absence of MalE using the interfacial positions 83 and 85 in the Q-loop, while no distance changes were observed between spin labels in the regulatory domain or attached at position 117 located at the outer surface in the vicinity of position 128 (29). Possibly, in the absence of MalE, binding of ATP to MalK slightly modifies only the Q-loop regions, leaving the overall ATP cassette dimer in an open state.

Under physiological conditions, it is assumed that the resting state of the transporter is ATP bound (30) and the MalK dimer is in an open conformation (Fig. 6*A*). Unliganded (open) or liganded (closed) MalE would then contact the transporter with both lobes inducing the full closure of the NBDs. When substrate is available, the up-regulation of *malE* expression assures that the closed (liganded) form, thus a productive cycle, will prevail (25). Following ATP hydrolysis, maltose is translocated to the cytoplasm, and upon dissociation of phosphate, the transporter might exchange the unliganded MalE with a closed liganded copy in the presence of maltose or with an open unliganded MalE if maltose is becoming unavailable in the environment (Fig. 6*C*).

These data, obtained by two independent experimental tools, working either at ambient temperature (cross-linking) or in a frozen environment (DEER), highlight the conformational plasticity of a type I ABC importer and expand the knowledge on binding protein–transporter interactions, which lead to coupling conformational changes to substrate translocation. One intriguing point is that this interaction is mediated by the extended second periplasmic loop (P2) of MalF, confined to maltose transporters from enteric bacteria and a few other prokaryotes. Thus, assuming a basically common mode of SBP–transporter interactions and

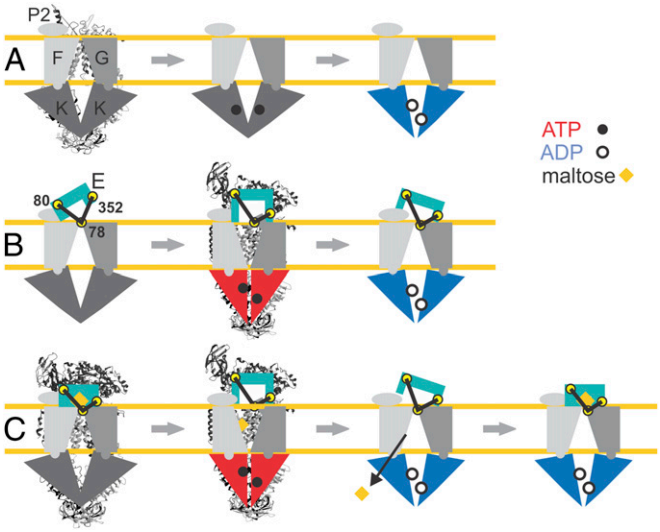

Fig. 6. Model for MalE–$MalFGK_2$ interaction during the nucleotide cycle. (*A*) $MalFGK_2$ alone during nucleotide cycle. Only ADP–Mg^{2+} is shown to affect the relative displacement of the NBDs. (*B*) $MalFGK_2$-E conformations during nucleotide cycle in the absence of maltose. The spin-labeled positions 78 in MalG, 80 in MalE (*N*-lobe), and 352 in MalE (C-lobe) are highlighted by yellow circles. (*C*) Nucleotide cycle in $MalFGK_2$-E associated with maltose translocation. The two experimentally detected ADP-states are presented as posthydrolytic states after translocation of maltose (open MalE) and upon loading of a new maltose-loaded closed MalE. The available X-ray structures of $MalFGK_2$ alone in the apo-state (PDB 3FH6) and $MalFGK_2$-E in the pre-translocation state (3PV0) and in the AMP–PNP-state (3PUY) are presented behind the corresponding schematic models.

transmembrane signaling, in the vast majority of canonical importers the periplasmic contact must be maintained differently. How this is achieved remains to be elucidated.

Materials and Methods

More details are provided in *SI Materials and Methods*.

Protein Expression, Purification, and Spin Labeling. Gene expression and purification of $MalFGK_2$ and of MalE were performed according to methods described elsewhere (17, 31, 32). Spin labeling of the transporter mutants was performed according to ref. 8. ATPase activity of all proteins was tested in detergent solution and in liposomes before and after spin labeling. Two selected cysteine mutants in MalG as well as the three supercomplex variants were tested for substrate transport in liposomes using [^{14}C] maltose.

Cross-Linking Experiments. Cross-linking experiments using homobifunctional thiosulfonate linkers were performed as described earlier (33).

DEER Experiments. Dipolar time evolution data were acquired using the four-pulse DEER experiment (34). DEER traces were measured either in a conventional X-band spectrometer (Bruker ELEXSYS-II E580) or in a homemade, high-power Q-band spectrometer equipped with a homemade oversized resonator (23).

ACKNOWLEDGMENTS. We thank Heidi Landmesser (Humboldt-Universität zu Berlin) for excellent technical assistance. E.B. and S.B. especially thank G. Jeschke (ETH Zurich) for fruitful discussions. This work was supported by the Deutsche Forschungsgemeinschaft (D-A-CH Grant SCHN 274/15-1 to E.S.) and the Swiss National Science Foundation (D-A-CH Grant 20PA21E-129361/1 to E.B.).

1. Davidson AL, Dassa E, Orelle C, Chen J (2008) Structure, function, and evolution of bacterial ATP-binding cassette systems. *Microbiol Mol Biol Rev* 72(2):317–364.
2. Moussatova A, Kandt C, O'Mara ML, Tieleman DP (2008) ATP-binding cassette transporters in *Escherichia coli*. *Biochim Biophys Acta* 1778(9):1757–1771.
3. Vasiliou V, Vasiliou K, Nebert DW (2009) Human ATP-binding cassette (ABC) transporter family. *Hum Genomics* 3(3):281–290.
4. Eitinger T, Rodionov DA, Grote M, Schneider E (2011) Canonical and ECF-type ATP-binding cassette importers in prokaryotes: Diversity in modular organization and cellular functions. *FEMS Microbiol Rev* 35(1):3–67.
5. Rees DC, Johnson E, Lewinson O (2009) ABC transporters: The power to change. *Nat Rev Mol Cell Biol* 10(3):218–227.
6. Locher KP (2009) Review. Structure and mechanism of ATP-binding cassette transporters. *Philos Trans R Soc Lond B Biol Sci* 364(1514):239–245.
7. Lewinson O, Lee AT, Locher KP, Rees DC (2010) A distinct mechanism for the ABC transporter BtuCD-BtuF revealed by the dynamics of complex formation. *Nat Struct Mol Biol* 17(3):332–338.
8. Grote M, et al. (2009) Transmembrane signaling in the maltose ABC transporter $MalFGK_2$-E: Periplasmic MalF-P2 loop communicates substrate availability to the ATP-bound MalK dimer. *J Biol Chem* 284(26):17521–17526.
9. Orelle C, Ayvaz T, Everly RM, Klug CS, Davidson AL (2008) Both maltose-binding protein and ATP are required for nucleotide-binding domain closure in the intact maltose ABC transporter. *Proc Natl Acad Sci USA* 105(35):12837–12842.
10. Davidson AL, Shuman HA, Nikaido H (1992) Mechanism of maltose transport in *Escherichia coli*: Transmembrane signaling by periplasmic binding proteins. *Proc Natl Acad Sci USA* 89(6):2360–2364.
11. Berntsson RP, Smits SH, Schmitt L, Slotboom DJ, Poolman B (2010) A structural classification of substrate-binding proteins. *FEBS Lett* 584(12):2606–2617.
12. Bordignon E, Grote M, Schneider E (2010) The maltose ATP-binding cassette transporter in the 21st century—Towards a structural dynamic perspective on its mode of action. *Mol Microbiol* 77(6):1354–1366.
13. Oldham ML, Khare D, Quiocho FA, Davidson AL, Chen J (2007) Crystal structure of a catalytic intermediate of the maltose transporter. *Nature* 450(7169):515–521.
14. Khare D, Oldham ML, Orelle C, Davidson AL, Chen J (2009) Alternating access in maltose transporter mediated by rigid-body rotations. *Mol Cell* 33(4):528–536.
15. Oldham ML, Chen J (2011) Crystal structure of the maltose transporter in a pre-translocation intermediate state. *Science* 332(6034):1202–1205.
16. Oldham ML, Chen J (2011) Snapshots of the maltose transporter during ATP hydrolysis. *Proc Natl Acad Sci USA* 108(37):15152–15156.
17. Daus ML, Grote M, Schneider E (2009) The MalF P2 loop of the ATP-binding cassette transporter $MalFGK_2$ from *Escherichia coli* and *Salmonella enterica serovar typhimurium* interacts with maltose binding protein (MalE) throughout the catalytic cycle. *J Bacteriol* 191(3):754–761.
18. Austermuhle MI, Hall JA, Klug CS, Davidson AL (2004) Maltose-binding protein is open in the catalytic transition state for ATP hydrolysis during maltose transport. *J Biol Chem* 279(27):28243–28250.
19. Merino G, Boos W, Shuman HA, Bohl E (1995) The inhibition of maltose transport by the unliganded form of the maltose-binding protein of *Escherichia coli*: Experimental findings and mathematical treatment. *J Theor Biol* 177(2):171–179.
20. Tang C, Schwieters CD, Clore GM (2007) Open-to-closed transition in apo maltose-binding protein observed by paramagnetic NMR. *Nature* 449(7165):1078–1082.
21. Gould AD, Telmer PG, Shilton BH (2009) Stimulation of the maltose transporter ATPase by unliganded maltose binding protein. *Biochemistry* 48(33):8051–8061.
22. Loo TW, Clarke DM (2001) Determining the dimensions of the drug-binding domain of human P-glycoprotein using thiol cross-linking compounds as molecular rulers. *J Biol Chem* 276(40):36877–36880.
23. Polyhach Y, et al. (2012) High sensitivity and versatility of the DEER experiment on nitroxide radical pairs at Q-band frequencies. *Phys Chem Chem Phys* 14(30): 10762–10773.
24. Polyhach Y, Bordignon E, Jeschke G (2011) Rotamer libraries of spin labelled cysteines for protein studies. *Phys Chem Chem Phys* 13(6):2356–2366.
25. Manson MD, Boos W, Bassford PJ, Jr., Rasmussen BA (1985) Dependence of maltose transport and chemotaxis on the amount of maltose-binding protein. *J Biol Chem* 260(17):9727–9733.
26. van der Heide T, Poolman B (2002) ABC transporters: One, two or four extracytoplasmic substrate-binding sites? *EMBO Rep* 3(10):938–943.
27. Biemans-Oldehinkel E, Poolman B (2003) On the role of the two extracytoplasmic substrate-binding domains in the ABC transporter OpuA. *EMBO J* 22(22):5983–5993.
28. Bao H, Duong F (2012) Discovery of an auto-regulation mechanism for the maltose ABC transporter $MalFGK_2$. *PLoS ONE* 7(4):e34836.
29. Grote M, et al. (2008) A comparative electron paramagnetic resonance study of the nucleotide-binding domains' catalytic cycle in the assembled maltose ATP-binding cassette importer. *Biophys J* 95(6):2924–2938.
30. Jensen KF, Dandanell G, Hove-Jensen B, Willemoes M (18 August 2008) Nucleotides, nucleosides, and nucleobases. *EcoSal-Escherichia coli and Salmonella: Cellular and Molecular Biology*, eds Böck A, et al. (ASM Press, Washington, DC).
31. Daus ML, Berendt S, Wuttge S, Schneider E (2007) Maltose binding protein (MalE) interacts with periplasmic loops P2 and P1 respectively of the MalFG subunits of the maltose ATP binding cassette transporter ($MalFGK_2$) from *Escherichia coli/Salmonella* during the transport cycle. *Mol Microbiol* 66(5):1107–1122.
32. Landmesser H, et al. (2002) Large-scale purification, dissociation and functional reassembly of the maltose ATP-binding cassette transporter ($MalFGK_2$) of *Salmonella typhimurium*. *Biochim Biophys Acta* 1565(1):64–72.
33. Daus ML, et al. (2007) ATP-driven MalK dimer closure and reopening and conformational changes of the "EAA" motifs are crucial for function of the maltose ATP-binding cassette transporter ($MalFGK_2$). *J Biol Chem* 282(31):22387–22396.
34. Pannier M, Veit S, Godt A, Jeschke G, Spiess HW (2000) Dead-time free measurement of dipole-dipole interactions between electron spins. *J Magn Reson* 142(2):331–340.
35. Jeschke G, et al. (2006) DEERAnalysis2006—A comprehensive software package for analyzing pulsed ELDOR data. *Appl Magn Reson* 30(3-4):473–498.